Sensors & Actuators: B. Chemical 321 (2020) 128508

Contents lists available at ScienceDirect

Sensors and Actuators B: Chemical

journal homepage: www.elsevier.com/locate/snb

3D-printed lab-in-a-syringe voltammetric cell based on a working electrode modified with a highly efficient Ca-MOF sorbent for the determination of Hg (II)

Christos Kokkinos[a,*], Anastasios Economou[a], Anastasia Pournara[b], Manolis Manos[b,c,**], Ioannis Spanopoulos[d], Mercouri Kanatzidis[d], Thomais Tziotzi[e], Valeri Petkov[f], Antigoni Margariti[g], Panagiotis Oikonomopoulos[g], Giannis S. Papaefstathiou[g,*]

[a] Laboratory of Analytical Chemistry, Department of Chemistry, National and Kapodistrian University of Athens, Athens 157 71, Greece
[b] Department of Chemistry, University of Ioannina, 45110 Ioannina, Greece
[c] University Research Center of Ioannina (URCI) - Institute of Materials Science and Computing, Greece
[d] Department of Chemistry, Northwestern University, Evanston, IL 60208, USA
[e] Department of Chemistry, University of Crete, Voutes 71003, Herakleion, Greece
[f] Department of Physics and Science of Advanced Materials Program, Central Michigan University, Mt. Pleasant, MI 48859, USA
[g] Laboratory of Inorganic Chemistry, Department of Chemistry, National and Kapodistrian University of Athens, Athens 157 71, Greece

ARTICLE INFO

Keywords:
Metal-organic frameworks
3D-printed electrode
Electrochemical sensing
Sorption
Mercury

ABSTRACT

This work combines, for the first time, 3D-printing technology and a highly efficient metal organic framework (Ca-MOF) as an electrode modifier to produce a novel fully integrated lab-in-a-syringe device for the sensitive determination of Hg(II) by anodic stripping voltammetry. The specific Ca-MOF ($[Ca(H_4L)(DMA)_2]\cdot 2DMA$ where H_6L is the *N,N'*-bis(2,4-dicarboxyphenyl)-oxalamide and DMA is the *N,N*-dimethylacetamide) shows an exceptional Hg(II) sorption capability over a wide pH range and its mechanism is elucidated via spectroscopic and X-ray diffraction studies. The voltammetric lab-in-a-syringe device is fabricated through a single-step process using a dual extruder 3D printer and is composed of a vessel integrating two thermoplastic conductive electrodes (serving as the counter and pseudo-reference electrodes) and of a small detachable 3D-printed syringe loaded with a graphite paste/Ca-MOF mixture (which serves as the working electrode). After optimization of the fabrication and operational variables, a limit of detection of 0.6 μg L^{-1} Hg(II) was achieved, which is comparable or lower than that of existing sensors (plastic 3D-printed, gold and MOF-based electrodes). The adoption of 3D printing technology in combination with the highly efficient Ca-MOF enables the fabrication of a simple, low-cost and sensitive electrochemical sensor for Hg(II), which is suitable for on-site applications.

1. Introduction

Heavy metals are non-biodegradable and accumulate in the human tissues mainly through the food chain, while they are toxic even at trace levels. Among them, mercury is extremely toxic as it damages many human organs and causes serious diseases like Minamata disease and congnitive disorder [1–3]. Due to the high toxicity of mercury, sensitive analytical methods are required, especially for samples of high consumption such as fish products and drinking water [4,5]. Commonly, spectrometric techniques [6–11] are applied to mercury determination but they require well-trained technicians and complex, expensive and bulky instrumentation, which restrict their on-site applications. On the other hand, anodic stripping voltammetry (ASV) has been established as a very competitive technique for heavy metals analysis, since it offers high analytical sensitivity combined with fast and simple protocols, as well as with inexpensive and portable instrumentation [12].

Gold electrodes are the commonest transducers for the ASV determination of Hg(II), as mercury undergoes underpotential deposition at gold surfaces which facilitates the accumulation process [13–19]. These electrodes are mainly produced through screen-printing and microfabrication procedures. However, these step-by-step fabrication approaches are time-consuming, produce waste and require bulky equipment and expensive materials (i.e. masks and screens, inks and metallic targets) [15,14–19]. On the contrary, three-dimensional (3D)

* Corresponding authors.
** Corresponding author at: Department of Chemistry, University of Ioannina, 45110 Ioannina, Greece.
E-mail addresses: christok@chem.uoa.gr (C. Kokkinos), emanos@uoi.gr (M. Manos), gspapaef@chem.uoa.gr (G.S. Papaefstathiou).

https://doi.org/10.1016/j.snb.2020.128508
Received 7 May 2020; Received in revised form 22 June 2020; Accepted 22 June 2020
Available online 27 June 2020

printing can address many of these drawbacks. 3D printing is an easy, quick, inexpensive and flexible process, which is based on the CAD design of the device and its printing by thermoplastic filaments which are heated to a semi-molten state via extruders. The key features of 3D-printing (desktop-sized equipment, extremely low capital and materials costs, high fabrication speed and reproducibility, flexibility in design, ease of operation, transferability, eco-friendliness) make it a viable alternative for the fabrication of electrochemical sensors [20–24], while recent works have demonstrated that 3D-printed electrodes can be applied to mercury monitoring [22,21–24].

Nowadays, materials that can perform the dual function of sorption and sensing of heavy metals are very attractive and, lately, metal organic frameworks (MOFs) have been successfully tested in this role [25–32]. MOFs are polymeric metal complexes consisting of metal ions or clusters interconnected via polytopic organic ligands and are considered a subclass of coordination polymers. MOFs present excellent features, such as porous structure with tunable pore sizes, variety of functional groups and adjustable chemical functionality [25–34]. Nevertheless, the use of MOFs as electrode materials/modifiers can be considered still unexplored, since only a few reports have appeared in the pertinent literature dealing with the voltammetric determination of heavy metals [26–32,34].

The main procedure for the fabrication of MOF-based electrodes follows a complex workflow based on drop-casting of a MOF on the surface of a glassy carbon electrode [27–31,34]. According to this protocol, before every electrochemical measurement, the electrode surface must undergo a multi-step pre-treatment and modification procedure, therefore, these MOF-based electrodes cannot be considered as stand-alone sensors. Regarding Hg(II) voltammetric determination at MOF-based electrodes, there are only two recent reports applying drop-casting on glassy carbon of a non “green” Cr-MOF and a Zr-MOF composite with graphene aerogel [27,34]. Except from the multistep construction, another significant drawback of the existing MOF-based sensors is that the electrochemical measurements are carried out in “large-volume” electrochemical cells using conventional “large-size” external reference and counter electrodes.

We reported a 2D Ca-MOF ($[Ca(H_4L)(DMA)_2]\cdot 2DMA$ where H_6L is the *N,N’*-bis(2,4-dicarboxyphenyl)-oxalamide and DMA is the *N,N*-dimethylacetamide) which is insoluble in aqueous media and presents sorption and exchanged properties towards several heavy metals cations [32,35]. Here we show that this Ca-MOF is a highly efficient Hg (II) sorbent with rapid sorption kinetics and motivated by these excellent features, we employ it as an electrode modifier and produce a novel 3D-printed lab-in-a-syringe device for Hg(II) determination. The device is entirely fabricated by a single-step approach using a dual extruder 3D printer and two different filaments (Fig. 1). The lab-in-a-syringe device is composed of a small cell printed from a non-conductive polylactic acid (PLA) filament and of two electrodes (serving as, counter (CE), pseudo-reference (RE)) printed on the sides of the vessel from a conductive carbon-based PLA filament. The device also contains a mini detachable 3D-printed syringe printed from non-conductive PLA filament and loaded with graphite paste (GP) modified with the Ca-MOF serves as the working electrode (WE), while a conductive plunger (printed from conductive PLA filament) establishes electric contact of the WE with the potentiostat. The WE surface can be renewed by applying slight pressure on the syringe plunger and removing the excess of the material at the tip of the syringe. The device exhibits enhanced electroanalytical characteristics and is applied to Hg(II) ASV determination in bottled water and spiked fish oil samples. Overall, this work is the first to combine a MOF as electrode modifier with 3D printing technology in order to develop a voltammetric device.

2. Experimental section

The reagents and apparatus, the synthesis of the Ca-MOF, the batch ion-exchange studies, the fabrication process of the 3D-printed sensor, the ASV measurement procedure and the treatment of fish oil and bottled water before their ASV analysis are described in the Supporting Information.

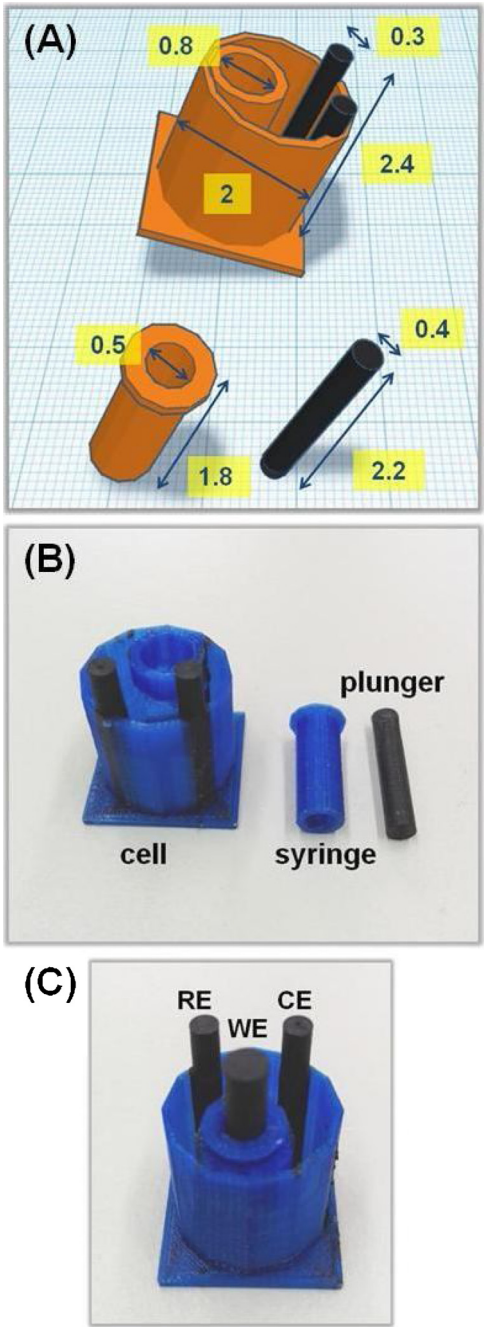

Fig. 1. (A) The dimensions of the 3D-printed lab-in-a-syringe cell (in cm). (B) Photograph of the main parts of the device. (C) Photograph of the complete device.

3. Results and discussion

3.1. Sorption study

3.1.1. Sorption kinetics

The sorption kinetics was determined through variable time sorption experiments. The results indicated that the capture of Hg(II) by Ca-MOF was remarkably fast, with ~ 92 % of the initial Hg(II) content (C_0 = 1 mg L^{-1}, pH ~7) removed within only 1 min Ca-MOF / solution

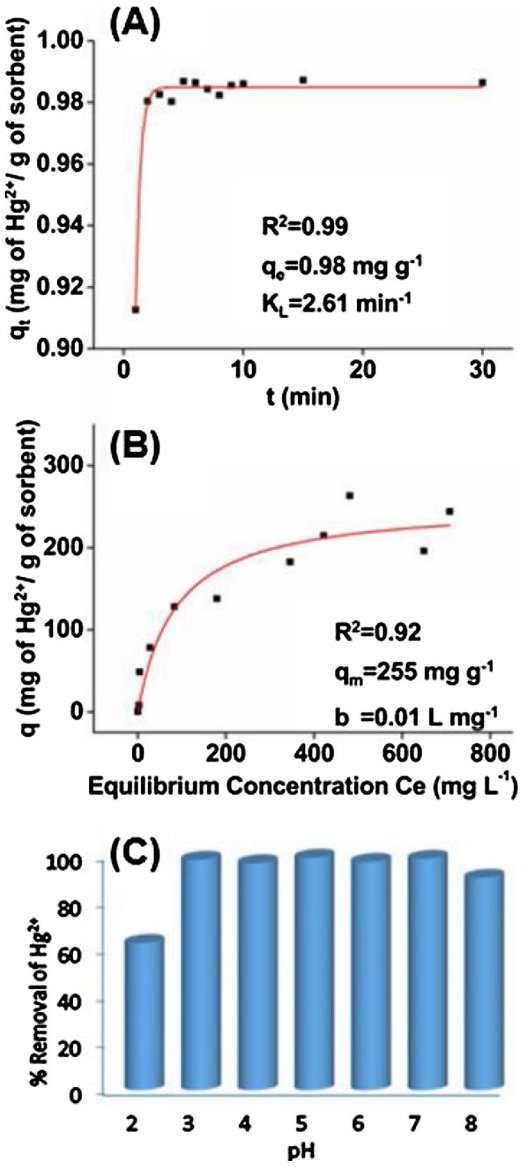

Fig. 2. (A) Fitting of the kinetics data with the Lagergren's first-order equation for the sorption of Hg(II) by the Ca-MOF. (B) Isotherm data for Hg(II) sorption by the Ca-MOF. The red line represents the fitting of the data with the Langmuir model. (C) Percentage (%) sorption of Hg(II) by the Ca-MOF at pH range 2-8 (initial concentration = 1 mg L^{-1}) (For interpretation of the references to colour in this figure legend, the reader is referred to the web version of this article).

contact (Fig. 2A). Interestingly, the sorption equilibrium was reached at the 2nd min of solution/ Ca-MOF contact with more than 98 % Hg(II) removed by Ca-MOF. The data can be fitted very well with the Lagergren's first order equation:

$$q_t = q_e[1 - \exp(-K_L t)]$$

where q_e = the amount (mg g^{-1}) of Hg(II) removed in equilibrium, K_L = the Lagergren or first-order rate constant (Fitting parameters: q_e = 0.98 ± 6.7 × 10^{-4} mg g^{-1}, K_L = 2.61 ± 0.03 min^{-1}, R^2 = 0.99) [36].

3.1.2. Sorption thermodynamics

The equilibrium analysis was needed to better understand the sorption process. The best fitting of the equilibrium sorption data of Hg (II) by the Ca-MOF was achieved by the Langmuir equation [37]:

$$q = q_m \frac{bC_e}{1 + bC_e}$$

where q (mg g^{-1}) is the amount of the Hg(II) sorbed at the equilibrium concentration C_e (mg L^{-1}), q_m is the maximum sorption capacity of the sorbent, b (L mg^{-1}) is the Langmuir constant related to the free energy of the sorption. The fitting of the data with the Langmuir model is shown in Fig. 2B.

The maximum sorption capacity was estimated to be 255 ± 24 mg Hg(II) (R^2 = 0.92) per g of Ca-MOF, which is close to the theoretically calculated sorption capacity for the sorption of one Hg(II) per formula unit (i.e. per one Ca^{2+}). The calculated q_m for Hg(II) sorption is 250 mg g^{-1} of Ca-MOF. A comparison of the Hg(II) sorption properties of Ca-MOF with those of state-of-the-art sorbents is provided in Table S1. Although several reported sorbents show higher maximum Hg(II) sorption capacities than that of Ca-MOF, the latter displays faster sorption capability and higher selectivity for Hg(II) (see below) vs. most of known materials.

3.2. Variable pH studies

The Ca-MOF MOF material was found to be capable to remove Hg (II) from aqueous solutions of a relatively wide pH range (pH = 2–8, Fig. 2C). Specifically, the capture of Hg(II) seems not to be influenced significantly at pH 3–8, with the percentage of Hg(II) removal to be higher than 91 %. At pH ~ 2, the Ca-MOF removed 63 % of the initial Hg(II) content (C_0 = 1 mg L^{-1}), indicating an efficient sorbent even under highly acidic conditions. Similar results were obtained from the electrochemical studies, discussed below.

3.3. Selectivity studies

The selectivity of Ca-MOF for Hg(II) vs. other heavy metals, such as Pb(II), Cd(II), Cu(II) was investigated in an aqueous solution containing 1 mg L^{-1} of each metal ion (pH = 7 ± 0.02). The sorption capacities of Ca-MOF were estimated to be 96.1 %, 71.4 % and 31.5 % for Hg(II), Pb(II) and Cd(II), respectively, while no Cu(II) removal was observed (Table S2). Furthermore, the selectivity of Ca-MOF for Hg(II) towards the aforementioned heavy metal ions was studied in natural spring water (intentionally contaminated by 1 mg L^{-1} of each metal ion), which contains common competitive non-toxic cations such as alkali and alkaline earth metal ions as well as several anions in relatively high concentrations (i.e. 93.1 mg L^{-1} Ca^{2+}, 1.9 mg L^{-1} Mg^{2+}, 2.6 mg L^{-1} Na^+ and 0.7 mg L^{-1} K^+, HCO_3^{2-} 299 mg L^{-1}, Cl- 8.7 mg L^{-1}, SO_4^{2-} 12 mg L^{-1}, NO_3- 7.9 mg L^{-1}, pH = 7 ± 0.02). The sorption capacities of Ca-MOF were determined 73 % and 77 %, for Hg(II) and Pb(II), respectively, but no sorption for Cd(II) and Cu(II) was observed (Table 1). Thus, the sorption efficiency of Ca-MOF for Hg(II) seems not to be influenced significantly from the presence of several competitive

Table 1
Selected results for Hg(II) sorption by the Ca-MOF.

Sample	C_0 (μg L^{-1})	C_e (μg L^{-1})	%removal
Hg(II)[a]	1000	20	98.0
Mixture of ions[a]	1000[b]	39 (Hg), 286 (Pb), 685 (Cd), 1000 (Cu)	96.1 (Hg), 71.4 (Pb), 31.5(Cd), 0 (Cu)
Mixture of ions[c]	1000[b]	270 (Hg), 230 (Pb), 1000 (Cu)	73 (Hg), 77 (Pb), 0 (Cu)

[a] Distilled water (pH = 7 ± 0.02).
[b] Initial concentration of each ion.
[c] Natural spring water with Ca^{2+} 93.1 mg L^{-1}, Mg^{2+} 1.9 mg L^{-1}, K^+ 0.7 mg L^{-1}, Na^+ 2.6 mg L^{-1}, HCO_3^{2-} 299 mg L^{-1}, Cl- 8.7 mg L^{-1}, SO_4^{2-} 12 mg L^{-1}, NO_3- 7.9 mg L^{-1}, pH = 7 ± 0.02).

cations, indicating Ca-MOF as an efficient sorbent and also promising for the remediation of real-world wastewater.

3.4. Characterization of Hg@CaMOF - mechanism of ion exchange

We employed a number of physical, spectroscopic and X-ray diffraction methods to characterize the Hg@Ca-MOF and gain insight into the possible mechanism of the Hg(II) sorption process. In our previous studies, it was clear that Ca-MOF was capable of exchanging the Ca^{2+} ions by other divalent metal ions, such as Pb(II), Cd(II), Ni(II), Zn(II) or Cu(II), when immersed in their aqueous solutions as evidenced by the absence of Ca^{2+} in the final M-MOFs [M(II) = Pb(II), Cd(II), Ni(II), Zn (II) or Cu(II)] materials [32,35]. Unlike our previous results, the Energy Dispersive Spectroscopy (EDS) analyses of the Hg@Ca-MOF indicated the presence of both Ca^{2+} and Hg(II) ions (Fig. S1) while the PXRD of the Hg@Ca-MOF (Fig. S2) was not informative, revealing low degree of crystallinity as a result of the particularly fast ion sorption process. In order to gain some insights on the nature of the Hg@Ca-MOF material we compared the IR spectra (Fig. S3) and TGA graphs (Fig. S4) with the respective data from all other M-MOFs [M(II) = Pb(II), Cd(II), Ni(II), Zn(II) or Cu(II)]. All IR spectra of the M-MOFs and Hg@Ca-MOF are missing the characteristic DMA bands and look similar but with noticeable differences. Indeed, none of the M-MOFs IR spectra matches perfectly the IR spectrum of Hg@Ca-MOF. The TGA graphs of the M-MOFs and that of Hg@Ca-MOF show that all materials contain various amounts of H_2O (weight losses at temperatures below 150 °C), while they are stable up to ~320 °C. After that temperature, they decompose, with the Hg@Ca-MOF exhibiting quite different decomposition profile than all other materials. Both IR and TGA indicate that Hg@Ca-MOF is quite different from all other M-MOF materials.

We also aimed at synthesizing new frameworks by reacting Hg(II) or mixtures of Hg(II) and Ca^{2+} with the oxalamide ligand, H_6L, in order to obtain indirect information about the material that resulted after the immersion of the Ca-MOF into the Hg(II) solutions. All attempts to isolate a mixed Hg(II)/Ca^{2+} product resulted in crystalline Ca-MOF as confirmed by obtaining the cell parameters from single-crystal x-ray data. However, the reaction of $HgCl_2$ with H_6L in a mixture of DMA/1,4-dioxane gave poorly diffracting single-crystals of $[Hg(H_4L)(DMA)_2]_n$ (synthetic details, crystallographic Table S2, crystal structure description and Figs. S5-S6 in the Supporting Information) which cannot be considered as a good model for the Hg@Ca-MOF since it comprises only Hg(II) while Hg@Ca-MOF comprises both Hg(II) and Ca^{2+} ions, as evidenced by the EDS.

Our final step to obtain structural information about the Hg@Ca-MOF was the use of high-energy XRD experiments coupled to atomic pair distribution function analysis (PDF). The experimental atomic PDFs (Fig. S7) show sharp peaks at low-r distances reflecting the presence of well-defined short-range atomic order and subsequent broad oscillations indicating the presence of medium-range atomic order. As can also be seen in Fig. S7, the atomic PDF for Hg@Ca-MOF is not similar to all other M-MOFs, neither matches the computed PDF of $[Hg(H_4L)(DMA)_2]_n$. Interestingly, the experimental PDF of Hg@Ca-MOF, does show two rather well-defined peaks in the vicinity of 2.4 and 2.8 Å. These peaks may be attributed to Ca-O and Hg-O distances, respectively.

All the above indicate that Hg@Ca-MOF is not similar to any of the other M-MOFs, since it comprises both Hg(II) and Ca^{2+} ions (as evidenced by the EDS analysis) while the rest of M-MOFs contain only a M (II) [M(II) = Pb(II), Cd(II), Ni(II), Zn(II) or Cu(II)] and no Ca^{2+}. The only possible explanation for this is that the pristine Ca-MOF when immersed in an aqueous solution of Hg(II) sorbs the targeted metal ion without losing the Ca^{2+}. This is possible only if the doubly deprotonated H_4L^{2-} in Ca-MOF deprotonates further (i.e. by becoming H_2L^{4-}) to stabilize the extra positive charge when Hg(II) is sorbed. Such mechanism of Hg(II) sorption is reminiscent of the Hg(II) capture by thiol-functionalized sorbents (such as mesoporous silica [38], clays [39] and MOFs [40]), which is accompanied by the deprotonation of the thiol groups accounting for the extra positive charge after the Hg(II) sorption.

3.5. Design and operational features of the 3D-Printed MOF-based sensor

The 3D-printing procedure was chosen for the fabrication of the syringe-cell device in order to minimize the fabrication and cost disadvantages of existing screen-printed and microfabricated sensors used for Hg(II) determination. In addition, the presented sensor overcomes the limitations of the existing MOF-based sensors such as the need for external electrodes and cells. To produce the MOF-based WE, we apply a simpler fabrication process than drop-casting. The applied protocol is based on the mixing of the appropriate small amount of MOF with graphite paste and the packing of mixture in the 3D-printed syringe. Following this process, ready-to-used sensors are produced, as the surface of the WE is renewed via a slight pressure on the syringe plunger. The cost of each device including the MOF (in terms of materials) is calculated at 0.264$ [bill of materials: conductive parts (2 electrodes and plunger): 0.022$, non-conductive parts (vessel and syringe): 0.045$, MOF: 0.176$, GP:0.021$)].

3.6. Optimization of MOF loading, supporting electrolyte, preconcentration potential and time

Different loadings of the Ca-MOF in the GP in the range 5–20 % (w/w) were compared for the determination of Hg(II) by SWASV (Fig. 3A). The response of unmodified GPE was very low and when the GPE was modified with the Ca-MOF the peak height of Hg(II) increased in accordance with the increase in the concentration of MOF. Besides, at modified Ca-MOF/GP electrodes better shaped stripping peaks were obtained than at unmodified GP electrode (Fig. 3B). It has been shown before that bare carbon-based electrodes exhibit low sensitivities and require higher preconcentration times for mercury determination [13,25,37]. As illustrated in Fig. 3A, the Ca-MOF/GPE at 10 % (w/w) presented approximately 6 times higher stripping peak height than the unmodified GPE, about 1.5 times higher sensitivity than that of 5 % (w/w) loading and almost similar peak height with that of 20 % (w/w) loading. Thus, a Ca-MOF/GPE at 10 % (w/w) was selected as the optimum loading combining lower consumption of Ca-MOF with better stripping response.

In addition, the effect of the supporting electrolyte was investigated by monitoring the stripping peak heights of Hg(II) at GPE modified with 10 % (w/w) Ca-MOF in different media: 0.100 mol L^{-1} acetate buffer (pH 4.5) and 0.100 − 0.001 mol L^{-1} hydrochloric acid. The 0.100 mol L^{-1} acetate buffer (pH 4.5) exhibited the best background response and high peak current of Hg(II) and thus it was selected as supporting electrolyte for the voltammetric experiments.

The effect of preconcentration potential on the stripping peak height of Hg(II) was tested in the range −1.0 to −0.1 V (with respect to carbon pseudo-RE) in a solution of 20 μg L^{-1} of Hg(II) (Fig. S8A). It was found that the stripping peak current of Hg(II) was high and almost constant at more negative potentials form −1.0 to −0.6 V, and then gradually decreased from −0.6 to −0.1 V. Thus, the preconcentation potential of -0.8 V was selected for further experiments.

The impact of electrolytic preconcentration time on the determination sensitivity of Hg(II) was also investigated in a solution containing 20 μg L^{-1} Hg(II). The stripping peak heights increased rapidly and almost linearly at low preconcentration times (from 60 − 360 s), while the increase rate of the peak current of Hg(II) was significant reduced when the preconcentration time was longer than 360 s (Fig. S8B). As a compromise between high sensitivity and short analysis times, a preconcentration time of 360 s was finally selected.

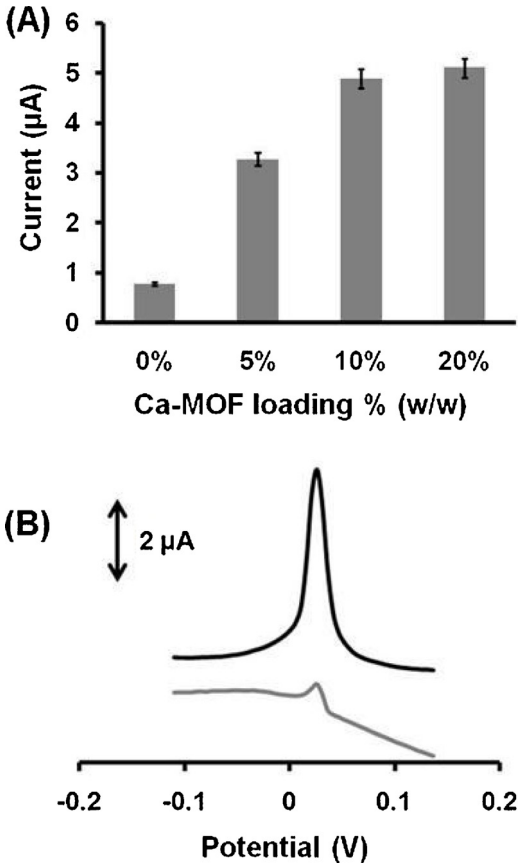

Fig. 3. (A) Effect of the concentration of the Ca-MOF at the GPE on the stripping peak current values of a solution containing 20 μg L^{-1} Hg(II). Each bar is the mean value ± sd (n = 3). (B) Comparative stripping voltammograms of a solution containing 20 μg L^{-1} Hg(II) at GPE modified with Ca-MOF (10 % w/w) (black line) and unmodified GPE (grey line) Supporting electrolyte: 0.100 mol L^{-1} acetate buffer (pH 4.5); preconcentration potential: -0.8 V; preconcentration time: 360 s.

3.7. Calibration features - Stability of the Ca-MOF sensor

Calibration for Hg(II) at various concentrations was performed at the Ca-MOF sensor using the following final conditions: supporting electrolyte: 0.100 mol L^{-1} acetate buffer (pH 4.5); preconcentration potential: −0.8 V; preconcentration time: 360 s; frequency: 50 Hz; pulse height:40 mV; step increment: 4 mV. The sensor exhibited a linear concentration dependence in the examined concentration range [2–40 μg L^{-1} for Hg(II)] with correlation coefficient (R^2) 0.996, as shown in Fig. 4. The limit of detection (LOD) was 0.6 μg L^{-1} (calculated using the equation LOD = 3sy/a, where sy is the standard deviation of the y residual of the calibration plot and a is the slope of the calibration plot). The LOD of the sensor compares well with that of gold modified electrodes [13,14,17,22] and is lower than that of plastic 3D-printed electrodes [23,24]. Compared with existing MOF-based electrodes for Hg(II) determination, the LOD of the Ca-MOF-sensor is lower than that obtained with the Cr-MOF electrode and comparable with that of the Zr-MOF/graphene electrode [27,34].

The repeatability of the Ca-MOF-based sensor was examined by assaying 20 μg L^{-1} Hg(II) for five repeated measurements and the % relative standard deviation (RSD%) was calculated at 3.8 %. Besides, three Ca-MOF/GPEs 10 % (w/w) were prepared for the determination of 20 μg L^{-1} Hg(II) and the RSD% of the measurements for the three sensors was 4.7 % (n = 3). These results showed satisfactory reproducibility of the syringe device. The stability of the sensor was also tested over a period of 2 months and a *t*-test demonstrated that the voltammetric response of the sensor remained statistically stable.

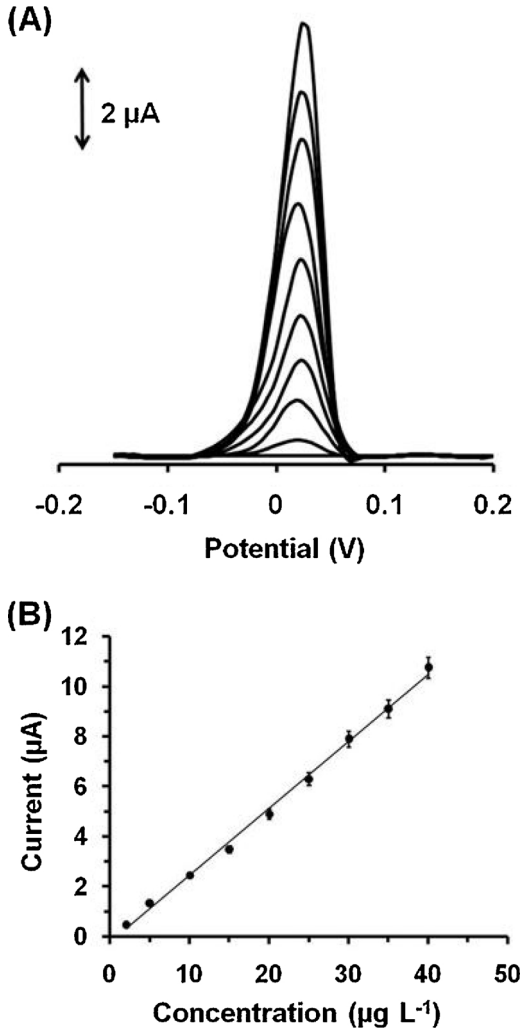

Fig. 4. (A) A series of SW voltammograms at the Ca-MOF/GPE (10 % w/w) for increasing concentrations of Hg(II). From below: blank, 2.0, 5.0 μg L^{-1} and 7 successive additions of 5.0 μg L^{-1} of Hg(II). (B) The corresponding calibration plot. Each bar is the mean value ± sd (n = 3). Supporting electrolyte: 0.100 mol L^{-1} acetate buffer (pH 4.5); preconcentration potential: −0.8 V; preconcentration time: 360 s.

3.8. Interference study

The effect of different heavy metals which may interfere with the determination of Hg(II) [i.e. Cu(II), Pb(II), Cd(II) and Zn(II)] on the stripping response of 20 μg L^{-1} of Hg(II) at the Ca-MOF/GPE was investigated. Pb(II), Cd(II) and Zn(II) did not interfere with the analysis of Hg(II) even at 10-fold higher concentrations over Hg(II). Cu(II) is generally considered as the major interferences in the determination of Hg(II) either on bare carbon-based electrodes [41] or gold-based electrodes [22,42], since this metal cation can readily preconcentrate on these sensors and present a stripping peak that may overlap with that of Hg(II). However, at the Ca-MOF/GPE in 0.100 mol L^{-1} acetate buffer (pH 4.5), Cu(II) presented a stripping peak which was well separated from the Hg peak (Fig. 5A).

3.9. Voltammetric analysis of real samples

In order to test the applicability of the syringe MOF-based sensors in the real sample analysis with complex matrices, the device was applied to the analysis of fish oil and a bottled water sample. In both samples the recovery was calculated by spiking the samples with Hg(II) [final concentration: 10 μg L^{-1} Hg(II)] and performing the analysis by the

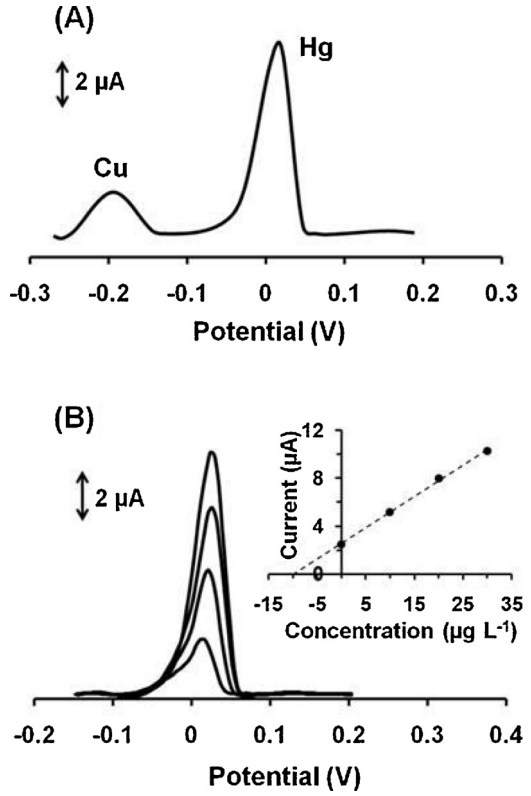

Fig. 5. (A) SW voltammogram at the Ca-MOF/GPE (10 % w/w) in a solution containing 10 μg L^{-1} of Cu(II) and 30 μg L^{-1} of Hg(II). (B) SW voltammograms for the determination of Hg(II) in spiked fish oil sample with 10 μg L^{-1} of Hg(II) at the Ca-MOF/GPE (10 % w/w). From below: spiked sample and 3 standard additions of 10 μg L^{-1} of Hg(II). (Inset) Standard additions curve. Supporting electrolyte: 0.100 mol L^{-1} acetate buffer (pH 4.5); preconcentration potential: −0.8 V; preconcentration time: 360 s.

standard addition method. A series of voltammograms after standard additions of Hg(II) in the fish oil sample is presented in Fig. 5B and the standard additions plot is depicted as an inset. The mean recovery for fish oil was 98 ± 5 % (n = 3) and for bottled water 101 ± 4 % (n = 3). These results indicate that the proposed device can be successfully applied to on-site monitoring of Hg(II) in complex samples.

4. Conclusions

In this work, a new integrated 3D-printed lab-in-a-syringe cell using a Ca-MOF as an electrode modifier was successfully developed for the ASV determination of Hg(II). The high sorption capability of the Ca-MOF enhances the sensitivity of the Hg(II) determination with a LOD of 0.6 μg L^{-1}, which is comparable or lower than that of existing sensors (plastic 3D-printed, gold and MOF-based electrodes). The Ca-MOF sensor is stable, reproducible and addresses the limitations of gold and MOF-based electrodes for Hg(II) determination in terms of cost, fabrication and operational simplicity. These features establish the Ca-MOF based 3D-printed lab-in-a-syringe device as an excellent candidate for simple and ultrasensitive determination of Hg(II) in complex matrices.

CRediT authorship contribution statement

Christos Kokkinos: Conceptualization, Investigation, Supervision, Visualization, Project administration, Resources, Writing - original draft, Writing - review & editing. **Anastasios Economou:** Resources, Writing - review & editing. **Anastasia Pournara:** Investigation, Writing - review & editing. **Manolis Manos:** Supervision, Project administration, Writing - review & editing, Resources. **Ioannis Spanopoulos:** Investigation. **Mercouri Kanatzidis:** Investigation, Resources. **Thomais Tziotzi:** Investigation, Resources. **Valeri Petkov:** Investigation, Resources. **Antigoni Margariti:** Investigation. **Panagiotis Oikonomopoulos:** Investigation. **Giannis S. Papaefstathiou:** Supervision, Project administration, Resources, Writing - review & editing.

Declaration of Competing Interest

The authors declare no competing financial interest. The work has not been published previously and it is not under consideration for publication elsewhere. Its publication is approved by all authors and tacitly or explicitly by the responsible authorities where the work was carried out, and that, if accepted, it will not be published elsewhere in the same form, in English or in any other language, including electronically without the written consent of the copyright holder.

Acknowledgment

This work was partially supported by the Special Account for Research Grants (SARG) of the National and Kapodistrian University of Athens (NKUA). The Bodossaki Foundation is gratefully acknowledged for donating the TGA to NKUA. The research work, by A. D. Pournara and M. J. Manos, was supported by the Hellenic Foundation for Research and Innovation (H.F.R.I.) under the “First Call for H.F.R.I. Research Projects to support Faculty members and Researchers and the procurement of high-cost research equipment grant” (Project Number: 348). Metal analysis was performed at the Northwestern University Quantitative Bio-element Imaging Center generously supported by NASA Ames Research Center NNA06CB93 G. MGK would like to acknowledge grant NSF DMR-1708254. This research used resources of the Advanced Photon Source, a U.S. Department of Energy (DOE) Office of Science User Facility operated for the DOE Office of Science by Argonne National Laboratory under Contract No. DE-AC02-06CH11357.

Appendix A. Supplementary data

Supplementary material related to this article can be found, in the online version, at doi:https://doi.org/10.1016/j.snb.2020.128508.

References

[1] C.M.L. Carvalho, E.-H. Chew, S.I. Hashemy, J. Lu, A. Holmgren, Inhibition of the human thioredoxin system, J. Biol. Chem. 283 (2008) 11913–11923, https://doi.org/10.1074/jbc.M710133200.
[2] T.W. Clarkson, L. Magos, The toxicology of mercury and its chemical compounds, Crit. Rev. Toxicol. 36 (2006) 609–662, https://doi.org/10.1080/10408440600845619.
[3] A.H. Stern, A review of the studies of the cardiovascular health effects of methylmercury with consideration of their suitability for risk assessment, Environ. Res. 98 (2005) 133–142, https://doi.org/10.1016/j.envres.2004.07.016.
[4] K.E. Levine, M.A. Levine, F.X. Weber, Y. Hu, J. Perlmutter, P.M. Grohse, Determination of mercury in an assortment of dietary supplements using an inexpensive combustion atomic absorption spectrometry technique, J. Autom. Methods Manag. Chem. 2005 (2005) 211–216, https://doi.org/10.1155/JAMMC.2005.211.
[5] N. Mei, B. Lai, J. Liu, X. Mao, G. Chen, Speciation of trace mercury impurities in fish oil supplements, Food Control 84 (2018) 221–225, https://doi.org/10.1016/j.foodcont.2017.08.001.
[6] P. Coufalík, O. Zvěřina, J. Komárek, Determination of mercury species using thermal desorption analysis in AAS, Chem. Pap. 68 (2014), https://doi.org/10.2478/s11696-013-0471-0.
[7] C. Kim, Characterization and speciation of mercury-bearing mine wastes using X-ray absorption spectroscopy, Sci. Total Environ. 261 (2000) 157–168, https://doi.org/10.1016/S0048-9697(00)00640-9.
[8] Y. Li, C. Chen, B. Li, J. Sun, J. Wang, Y. Gao, Y. Zhao, Z. Chai, Elimination efficiency of different reagents for the memory effect of mercury using ICP-MS, J. Anal. At. Spectrom. 21 (2006) 94–96, https://doi.org/10.1039/B511367A.
[9] D.E. León-Pérez, A.M. Muñoz-Jiménez, C. Jiménez-Cartagena, Determination of Mercury Species in Fish and Seafood by Gas Chromatography-Mass Spectrometry: Validation Study, Food Anal. Method. 8 (2015) 2383–2391, https://doi.org/10.

1007/s12161-015-0120-z.
[10] J. Li, W. Lu, J. Ma, L. Chen, Determination of mercury(II) in water samples using dispersive liquid-liquid microextraction and back extraction along with capillary zone electrophoresis, Microchim. Acta 175 (2011) 301–308, https://doi.org/10.1007/s00604-011-0679-z.
[11] N. Bi, Y. Chen, H. Qi, X. Zheng, Y. Chen, X. Liao, H. Zhang, Y. Tian, Spectrophotometric determination of mercury(II) ion using gold nanorod as probe, Sensor Actuat. B-Chem. 166–167 (2012) 766–771, https://doi.org/10.1016/j.snb.2012.03.068.
[12] A. Economou, C. Kokkinos, Advances in stripping analysis of metals, in: D.W.M. Arrigan (Ed.), RSC Detection Science Series No. 6, Electrochemical Strategies in Detection Science, 2016, pp. 1–18, , https://doi.org/10.1039/9781782622529-00001.
[13] D. Martín-Yerga, A. Costa-García, Recent advances in the electrochemical detection of mercury, Curr. Opin. Electrochem. 3 (2017) 91–96, https://doi.org/10.1016/j.coelec.2017.06.012.
[14] M. Zaib, M.M. Athar, A. Saeed, U. Farooq, Electrochemical determination of inorganic mercury and arsenic-A review, Biosens. Bioelectron. 74 (2015) 895–908, https://doi.org/10.1016/j.bios.2015.07.058.
[15] T.F. Tormin, G.K.F. Oliveira, E.M. Richter, R.A.A. Munoz, Voltammetric determination of Pb, Cu and Hg in biodiesel using gold screen-printed electrode: comparison of batch-injection analysis with conventional electrochemical systems, Electroanalysis 28 (2015) 940–946, https://doi.org/10.1002/elan.201501012.
[16] E. Fernández, L. Vidal, A. Costa-García, A. Canals, Mercury determination in urine samples by gold nanostructured screen-printed carbon electrodes after vortex-assisted ionic liquid dispersive liquid–liquid microextraction, Anal. Chim. Acta 915 (2016) 49–55, https://doi.org/10.1016/j.aca.2016.02.028.
[17] A.L. Squissato, D.P. Rocha, E.S. Almeida, E.M. Richter, R.A.A. Munoz, Stripping voltammetric determination of mercury in fish oil capsules using a screen-printed gold electrode, Electroanalysis. 30 (2017) 20–23, https://doi.org/10.1002/elan.201700570.
[18] E. Roditi, M. Tsetsoni, C. Kokkinos, A. Economou, Integrated on-chip sensor with sputtered Ag-Au-Au electrodes for the voltammetric determination of trace Hg(II), Sensor Actuat. B-Chem. 286 (2019) 125–130, https://doi.org/10.1016/j.snb.2019.01.136.
[19] C. Chen, J. Zhang, Y. Du, X. Yang, E. Wang, Microfabricated on-chip integrated Au–Ag–Au three-electrode system for in situ mercury ion determination, Analyst 135 (2010) 1010–1014, https://doi.org/10.1039/B924545F.
[20] A. Ambrosi, M. Pumera, 3D-printing technologies for electrochemical applications, Chem. Soc. Rev. 45 (2016) 2740–2755, https://doi.org/10.1039/c5cs00714c.
[21] H.H. Hamzah, S.A. Shafiee, A. Abdalla, B.A. Patel, 3D printable conductive materials for the fabrication of electrochemical sensors: a mini review, Electrochem. commun. 96 (2018) 27–31, https://doi.org/10.1016/j.elecom.2018.09.006.
[22] V. Katseli, N. Thomaidis, A. Economou, C. Kokkinos, Miniature 3D-printed integrated electrochemical cell for trace voltammetric Hg(II) determination, Sensor Actuat, BChem 308 (2020) 127715, , https://doi.org/10.1016/j.snb.2020.127715.
[23] V. Katseli, A. Economou, C. Kokkinos, Single-step fabrication of an integrated 3D-printed device for electrochemical sensing applications, Electrochem. commun. 103 (2019) 100–103, https://doi.org/10.1016/j.elecom.2019.05.008.
[24] J.G. Walters, S. Ahmed, I.M. Terrero Rodríguez, G.D. O'Neil, Trace analysis of heavy metals (Cd, Pb, Hg) using native and modified 3D printed graphene/poly(lactic acid) composite electrodes, Electroanalysis 32 (2020) 859–866, https://doi.org/10.1002/elan.201900658.
[25] A.D. Pournara, G.D. Tarlas, G.S. Papaefstathiou, M.J. Manos, Chemically modified electrodes with MOFs for the determination of inorganic and organic analytes via voltammetric techniques: a critical review, Inorg. Chem. Front. 6 (2019) 3440–3455, https://doi.org/10.1039/C9QI00965E.
[26] M. Roushani, A. Valipour, Z. Saedi, Electroanalytical sensing of Cd^{2+} based on metal–organic framework modified carbon paste electrode, Sensor Actuat. B-Chem. 233 (2016) 419–425, https://doi.org/10.1016/j.snb.2016.04.106.
[27] D. Wang, Y. Ke, D. Guo, H. Guo, J. Chen, W. Weng, Facile fabrication of cauliflower-like MIL-100(Cr) and its simultaneous determination of Cd^{2+}, Pb^{2+}, Cu^{2+} and Hg^{2+} from aqueous solution, Sensor Actuat. B-Chem. 216 (2015) 504–510, https://doi.org/10.1016/j.snb.2015.04.054.
[28] F. Cai, Q. Wang, X. Chen, W. Qiu, F. Zhan, F. Gao, Q. Wang, Selective binding of Pb^{2+} with manganese-terephthalic acid MOF/SWCNTs: theoretical modeling, experimental study and electroanalytical application, Biosens. Bioelectron. 98 (2017) 310–316, https://doi.org/10.1016/j.bios.2017.07.007.
[29] H. Guo, Z. Zheng, Y. Zhang, H. Lin, Q. Xu, Highly selective detection of Pb^{2+} by a nanoscale Ni-based metal–organic framework fabricated through one-pot hydrothermal reaction, Sensor Actuat. B-Chem. 248 (2017) 430–436, https://doi.org/10.1016/j.snb.2017.03.147.
[30] H. Guo, D. Wang, J. Chen, W. Weng, M. Huang, Z. Zheng, Simple fabrication of flake-like NH_2-MIL-53(Cr) and its application as an electrochemical sensor for the detection of Pb^{2+}, Chem. Eng. J. 289 (2016) 479–485, https://doi.org/10.1016/j.cej.2015.12.099.
[31] Y. Wang, L. Wang, W. Huang, T. Zhang, X. Hu, J.A. Perman, S. Ma, A metal–organic framework and conducting polymer based electrochemical sensor for high performance cadmium ion detection, J. Mater. Chem. A 5 (2017) 8385–8393, https://doi.org/10.1039/C7TA01066D.
[32] A.D. Pournara, A. Margariti, G.D. Tarlas, A. Kourtelaris, V. Petkov, C. Kokkinos, A. Economou, G.S. Papaefstathiou, M.J. Manos, A Ca^{2+} MOF combining highly efficient sorption and capability for voltammetric determination of heavy metal ions in aqueous media, J. Mater. Chem. A 7 (2019) 15432–15443, https://doi.org/10.1039/C9TA03337H.
[33] L. Fotouhi, M. Naseri, Recent electroanalytical studies of metal-organic frameworks: a mini-review, Crit. Rev. Anal. Chem. 46 (2015) 323–331, https://doi.org/10.1080/10408347.2015.1063978.
[34] M. Lu, Y. Deng, Y. Luo, J. Lv, T. Li, J. Xu, S.-W. Chen, J. Wang, Graphene aerogel–metal–organic framework-based electrochemical method for simultaneous detection of multiple heavy-metal ions, Anal. Chem. 91 (2018) 888–895, https://doi.org/10.1021/acs.analchem.8b03764.
[35] A. Margariti, S. Rapti, A.D. Katsenis, T. Friščić, Y. Georgiou, M.J. Manos, G.S. Papaefstathiou, Cu^{2+} sorption from aqueous media by a recyclable Ca^{2+} framework, Inorg. Chem. Front. 4 (2017) 773–781, https://doi.org/10.1039/C6QI00542J.
[36] A. Benhammou, A. Yaacoubi, L. Nibou, B. Tanouti, Adsorption of metal ions onto Moroccan stevensite: kinetic and isotherm studies, J. Colloid Interface Sci. 282 (2005) 320–326, https://doi.org/10.1016/j.jcis.2004.08.168.
[37] M.J. Manos, M.G. Kanatzidis, Sequestration of heavy metals from water with layered metal sulfides, Chem. Eur. J. 15 (2009) 4779–4784, https://doi.org/10.1002/chem.200900353.
[38] X. Feng, G.E. Fryxell, L.-Q. Wang, A.Y. Kim, J. Liu, K.M. Kemner, Functionalized monolayers on ordered mesoporous supports, Science 276 (1997) 923–926, https://doi.org/10.1126/science.276.5314.923.
[39] I.L. Lagadic, M.K. Mitchell, B.D. Payne, Highly effective adsorption of heavy metal ions by a thiol-functionalized magnesium phyllosilicate clay, Environ. Sci. Technol. 35 (2001) 984–990, https://doi.org/10.1021/es001526m.
[40] K.K. Yee, N. Reimer, J. Liu, S.Y. Cheng, S.M. Yiu, J. Weber, N. Stock, Z. Xu, Effective mercury sorption by thiol-laced metal–organic frameworks: in strong acid and the vapor phase, J. Am. Chem. Soc. 135 (2013) 7795–7798, https://doi.org/10.1021/ja400212k.
[41] J. Švarc-Gajić, Z. Stojanović, Z. Suturović, N. Marjanović, S. Kravić, Direct mercury determination in natural waters by chronopotentiometric stripping analysis in macroelectrode process vessel, Desalination 249 (2009) 253–259, https://doi.org/10.1016/j.desal.2008.08.018.
[42] M.C. Radulescu, A. Danet, Mercury determination in fish samples by chronopotentiometric stripping analysis using gold electrodes prepared from recordable CDs, Sensors 8 (2008) 7157–7171, https://doi.org/10.3390/s8117157.

Dr. Christos Kokkinos is Assistant Professor at the Department of Chemistry, National and Kapodistrian University of Athens (NKUA), Greece. His research interests include the fabrication of electrochemical sensors and biosensors and the development of analytical methods for (bio)chemical sensing.

Dr. Anastasios Economou is Professor at the Department of Chemistry, NKUA, Greece. His research focuses on electrochemical sensors and detection, automation in analysis, analytical chemiluminescence and separation techniques.

Dr. Anastasia Pournara received her PhD in Inorganic Chemistry from the University of Ioannina (UI), Greece. Her research is focused on the synthesis of MOFs with interesting ion exchange properties towards organic dyes and heavy metals.

Dr. Manolis Manos is an Associate Professor of Inorganic Chemistry at UI, Greece. His research interests are directed toward materials and composites with applications in water treatment and luminescence sensing.

Dr. Ioannis Spanopoulos is currently post-doctoral researcher at Northwestern University. His research interests include synthesis and study of MOFs as well as hybrid perovskite compounds with electronic and optoelectronic applications.

Dr. Mercouri Kanatzidis is the Charles E. and Emma H. Morrison Professor of Chemistry at Northwestern University. His research interests include chalcogenide materials and study of their properties as well as perovskite halides with applications in solid state solar cells and photonics.

Dr. Thomais Tziotzi is a post-doctoral fellow in the Laboratory of Inorganic Chemistry, at the Department of Chemistry at the University of Crete. Her research interests are mainly focused on the synthesis and characterization of polynuclear complexes by means of single-crystal crystallography and magnetic techniques.

Dr. Valeri Petkov is a Professor in the Department of Physics at Central Michigan University. His research interests include applied crystallography, X-ray (synchrotron) diffraction and structure determination and modeling.

Dr. Antigoni Margariti received her PhD in Inorganic Chemistry from the Department of Chemistry of NKUA. Her research focused on the synthesis and characterization of MOFs with interesting ion-exchange and electronic properties.

Panagiotis Oikonomopoulos is a PhD candidate in the Laboratory of Inorganic Chemistry of the NKUA, Greece. He is majoring in the development of new MOFs.

Dr. Giannis S. Papaefstathiou is Associate Professor of Inorganic Chemistry, NKUA, Greece. His research focuses on aspects of coordination chemistry and supramolecular chemistry.